ACS OMEGA

http://pubs.acs.org/journal/acsodf

Article

Copper Nanoparticle Loading and F Doping of Graphene Aerogel Enhance Its Adsorption of Aqueous Perfluorooctanoic Acid

Longfei Liu, Naiju Che, Shengsen Wang, Yanli Liu,* and Chengliang Li*

Cite This: *ACS Omega* 2021, 6, 7073−7085

Read Online

ACCESS | Metrics & More | Article Recommendations | Supporting Information

ABSTRACT: Perfluorooctanoic acid (PFOA) persists in the environment for a long time due to its stable physical and chemical properties, and it is harmful to the environment and biological system. In order to effectively remove PFOA from aqueous solution, Cu nanoparticles and fluorine-modified graphene aerogel (Cu/F-rGA) were fabricated by the microbubble template method. Compared with unmodified aerogels (rGA), the adsorption rate of PFOA on Cu/F-rGA was enhanced 2.68-fold. These significant improvements were assumed to benefit from the ligand exchange reaction and hydrophobic and F−F interactions. The regeneration of Cu/F-rGA maintained 73.26% with ethanol as the desorption solvent after 10 times adsorption−desorption. The fitting results of the statistical physics model showed that PFOA tended to be parallel to the adsorption site at low temperature and perpendicular at high temperature. The number of PFOA molecules connected to each adsorption site was 0.53 to 1.41, and the number of adsorption layers of PFOA on the Cu/F-rGA was between 1.63 and 2.51. Compared with the response surface methodology and artificial neural network, an adaptive neuro-fuzzy inference system had more accurate analysis and prediction results. These results provide an effective and alternative strategy to remove PFOA from aqueous solution with environment-friendly consumption.

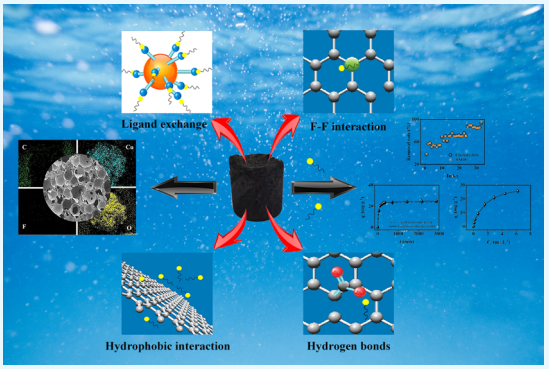

1. INTRODUCTION

Per- and polyfluoroalkyl substances (PFASs) are a series of synthetic organic chemicals and are widely used in industrial and consumer products.[1−4] PFOA is one of the most stable PFASs, and some long-chain PFASs and precursors can form PFOA after degradation.[5] However, due to its specific physical and chemical properties (Table S1), PFOA persists in the environment for a long time without being degraded by various approaches. This led to the concentration of PFOA in some environmental media, especially in water environments, reaching the level of $\mu g\ L^{-1}$ or even mg L^{-1}.[6] Therefore, PFOA is transferred and circulated in the ecosystem through various media. For example, PFOA could be detected in soil, water, plants, and even polar glaciers in the environment.[7−10] This is a serious threat to the health of organisms and humans.[11,12] Therefore, it is an urgent task to effectively remove PFOA from an aqueous medium, especially from tap water.

Nowadays, the traditional treatment methods, such as the flocculation, sand filtration, catalysis, and so on, were widely used to remove PFOA in water.[13−19] However, the effect of these methods was not optimistic, or some harmful intermediate products were produced, which limited their large-scale application.[20] The adsorption method has the advantages of low cost, simple operation, high efficiency, and environmental friendliness and has been widely used to remove pollutants in aqueous solutions. Traditional adsorbents, such as activated carbon and mineral materials, can absorb PFOA from high-concentration wastewater.[21,22] However, the adsorption efficiency of these adsorbents was not as high as expected.[23] Therefore, it is necessary to develop novel adsorption materials or technologies with a high adsorption capacity and high adsorption rate.

Some studies found that the adsorption capacity of PFOA on carbon-based materials such as biochar or carbon nanotubes was higher than that of minerals and sediment.[3,24−26] This was due to the excellent hydrophobicity of carbon nanotubes and biochar. In addition, metal nanoparticles (i.e., zero-valent iron, Fe_2O_3, and Fe_3O_4) had an outstanding removal effect on PFOA.[27−30] Complex exchange and hydrogen bonding played indelible roles in this process.[31−33] However, the particle sizes of carbon nanotubes and metal nanoparticles were so fine that they need high-speed centrifugal separation or filtration to achieve solid−liquid

Received: January 4, 2021
Accepted: February 23, 2021
Published: March 4, 2021

https://dx.doi.org/10.1021/acsomega.1c00044
ACS Omega 2021, 6, 7073−7085

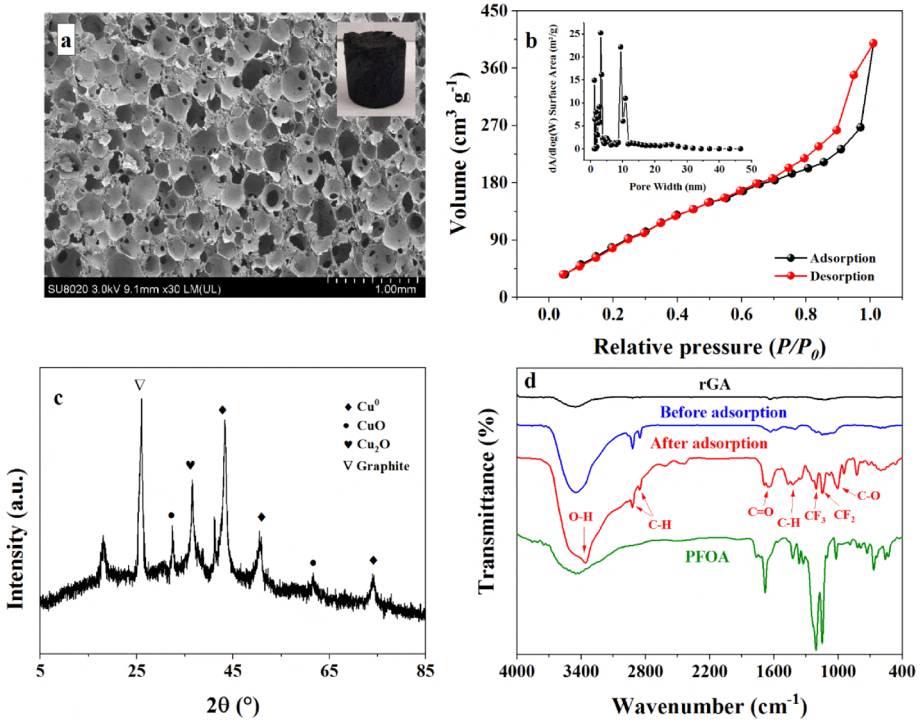

Figure 1. Characterization of Cu/F-rGA. (a) SEM, (b) nitrogen adsorption−desorption isotherms of Cu/F-rGA (inset: the corresponding pore size distribution curves), (c) XRD patterns, and (d) FTIR spectra before and after the adsorption.

separation.[31] Likewise, this caused great resistance to industrial promotion.

Graphene oxide (GO) has abundant oxygen-containing functional groups and has high dispersity and functionality in aqueous media. In addition, GO is ideal as a starting material for the preparation of functional materials such as aerogel because the oxygen moieties presence on the basal plane and edges can covalently react with different compounds.[34] Compared with the adsorbent with a loose structure, the stable three-dimensional structure of aerogel makes it possible to achieve solid−liquid separation through simple filtration after equilibrium adsorption. This greatly simplifies the separation process and reduces the operation cost.[34] The network of aerogel possesses a high surface area, low density, and high porosity, which makes it have great application potential in the treatment of pollutants.[35]

Based on previous research studies, carbon nanotubes loaded with metal nanoparticles improved their adsorption capacity for PFOA.[31,36] In addition, the F−F interaction had a positive effect on the removal of PFASs.[37] Therefore, in this study, it is hypothesized that the graphene aerogel loaded with Cu nanoparticles (Cu NPs) and doped with F elements can increase the adsorption capacity of PFOA. That is, the F element was doped into the graphene structure first, and then the three-dimensional aerogel was prepared by the micro-bubble template method. Finally, the Cu NPs were loaded onto the aerogel. The modified aerogel was used to study the adsorption behaviors of PFOA through adsorption kinetics, isotherms, and the influence of environmental factors and comprehensively evaluate the adsorption potential and application value of the aerogel to PFOA.

2. RESULTS AND DISCUSSION

2.1. Characterization of Cu/F-rGA. In order to be used in different environments, Cu/F-rGA needs a stable structure. After equilibrating in different pH values (4, 7, and 10), ionic strengths (10, 50, and 100 mM), and liquid media (ethanol, acetone, and chloroform) for 48 h, Cu/F-rGA still maintained its original shape and did not spread into the medium (Figure S1). This showed that Cu/F-rGA can remove PFOA in different liquid environments. Figure 1a exhibits the SEM image of Cu/F-rGA. It had a honeycomb structure with a diameter of 100−250 μm. This structure can greatly improve the stability of the three-dimensional structure of Cu/F-rGA.[38]

Figure 1b shows the nitrogen adsorption−desorption isotherms of Cu/F-rGA. The obvious H3 hysteresis loops indicated that Cu/F-rGA had a rich mesoporous structure.[39] This was conducive to the diffusion of solution inside Cu/F-rGA. In addition, the embedded graph in Figure 1b showed that the pore size of Cu/F-rGA ranged from 1.18 to 14.76 nm, and it mainly contains micropores (1.27 nm) and mesopores (3.43 nm). The physical and chemical properties of the prepared aerogels are listed in Table S2. The results showed that the specific surface area (SSA) of F-rGA was improved by doping an F element. This was attributed to the fact that the doping of the F element increased the spacing of graphene sheets.[40] However, the SSA of Cu/F-rGA was smaller than that of other aerogels. This was mainly due to the load of Cu NPs, which caused partial pore size of the aerogel to be blocked.

In the XRD pattern of Cu/F-rGA, the diffraction peaks of Cu NPs (JCPDS card no. 04-0836) appeared at 43.3, 50.5, and 74.3° (Figure 1c), respectively. In addition, the diffraction peaks of CuO (JCPDS card no. 05-0661) appeared at 32.4 and 61.7°. The possible cause of CuO was that Cu NPs were oxidized in air. A graphite diffraction peak of rGO appeared at 2θ = 25.8°. This was because GO was reduced to form rGO under the action of L-ascorbic acid. In addition, the results of EDS in Figure S2 showed that C, O, F, and Cu elements were distributed on Cu/F-rGA. This indicated that the F element

https://dx.doi.org/10.1021/acsomega.1c00044
ACS Omega 2021, 6, 7073−7085

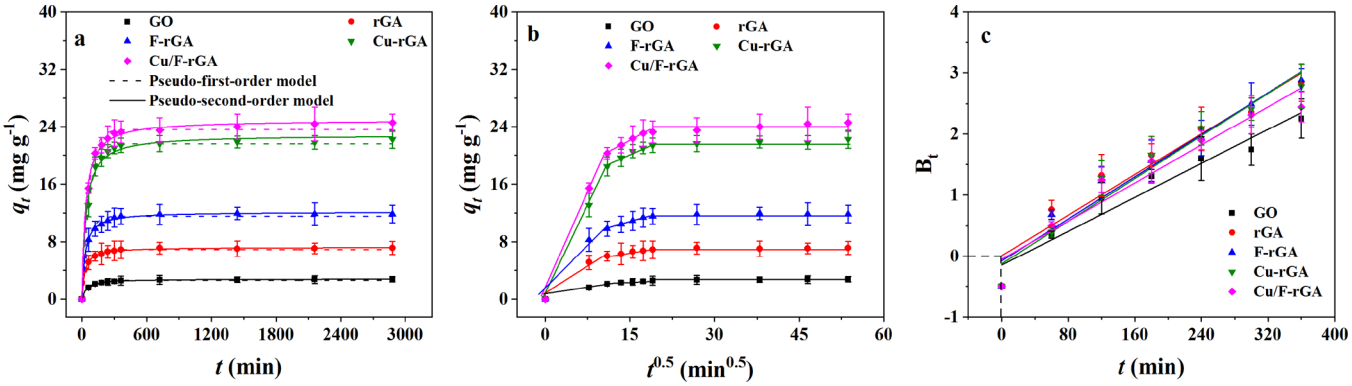

Figure 2. Adsorption kinetic data of PFOA on GO, rGA, F-rGA, Cu-rGA, and Cu/F-rGA were fitted by (a) pseudo-first-order model and pseudo-second-order models, (b) intraparticle diffusion model, and (c) Boyd model.

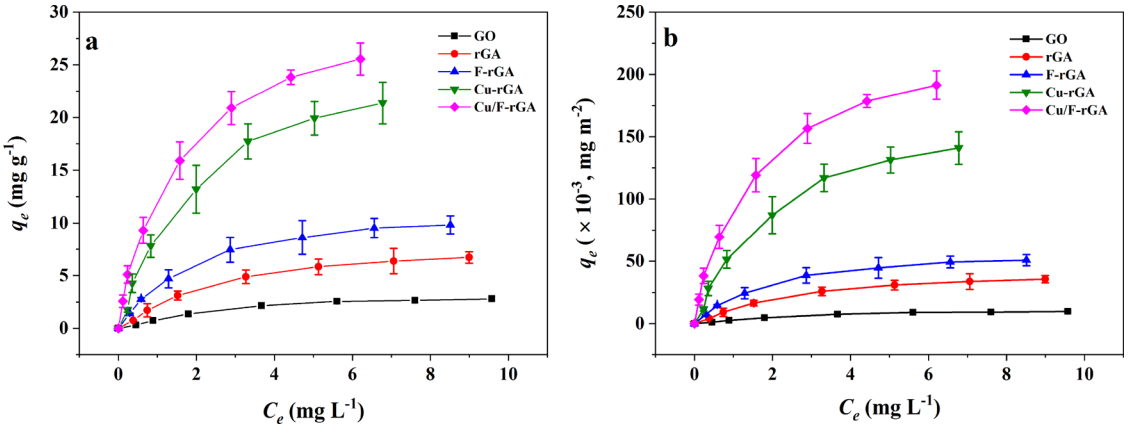

Figure 3. Adsorption isotherm data of PFOA on (a) GO, rGA, F-rGA, Cu-rGA, and Cu/F-rGA, and (b) normalized by the specific surface area.

was doped on the graphene, and the Cu NPs were also loaded on the aerogel.

Functional groups of Cu/F-rGA were identified by the FTIR spectrum and are exhibited in Figure 1d and Figure S3b. The peak at 1420 cm^{-1} was ascribed to the C−F bond because F atoms were doped on graphite.[41] The band appeared at 3432 cm^{-1} was due to the stretching of O−H. This attributed to the coordination between OH and Cu NPs.[42] The peaks at 528 and 559 cm^{-1} were the characteristic peaks of Cu−O, belonging to Cu−OH and CuO, respectively.[43]

2.2. Adsorption Trait. *2.2.1. Adsorption Kinetics.* Figure 2 shows the adsorption kinetics of PFOA on GO and the aerogels, and the results were fitted by different models. It was clearly seen in Figure 2a that PFOA was rapidly transferred to the aerogel surface at the initial 60 min. In the next 60−360 min, PFOA slowly diffused into the aerogels and then reached the equilibrium of adsorption (>360 min). In the initial stage, there were a large number of adsorption sites on the surface of the aerogels, which rapidly bound PFOA in the solution.[31] As the adsorption proceeded, PFOA diffused into the aerogels, and the available effective adsorption sites gradually decreased. Therefore, the adsorption rate decreased, and the adsorption equilibrium gradually reached. Relatively speaking, the adsorption process of PFOA on GO was shorter than this time. This was mainly because GO had a loose structure, and there was no barrier or obstacle to the PFOA diffusion.

In order to understand the adsorption process in detail, four different kinetic models were used to fit the transient behavior of the adsorption process. By comparing the correlation coefficient r^2, the pseudo-second-order model was more suitable to describe the adsorption behavior of PFOA on Cu/F-rGA. This showed that the adsorption process involved both physical and chemical adsorption. The initial adsorption rate (ν_0) of PFOA on Cu/F-rGA was 0.7813 mg g^{-1} min^{-1}, which was 2.68 times of that of rGA (Table S3). It indicated that the adsorption rate was improved by grafted F elements and Cu NPs. As reported, the rate constants of bamboo-derived activated carbon and Fe_3O_4 nanoparticle-loaded activated carbon were around 2.62 × 10^{-5} and 3.94 × 10^{-4} g mg^{-1} min^{-1}, respectively.[32,44] Cu/F-rGA showed a higher adsorption rate, which may be related to its more regular pore structure than activated carbon. The fitting results of the intraparticle diffusion model (Figure 2b) and Boyd model (Figure 2c) also showed that intraparticle diffusion was the main rate control step of PFOA adsorption on rGA, while the adsorption rates of PFOA on F-rGA, Cu-rGA, and Cu/F-rGA were controlled by both boundary diffusion and intraparticle diffusion.[31]

2.2.2. Adsorption Isotherms. The adsorption of PFOA on aerogels is shown in Figure 3. The results in Figure 3a showed that the adsorption capacity of PFOA on Cu/F-rGA was significantly higher than that of the control group. For example, when the equilibrium concentration of PFOA was 2 mg L^{-1}, the adsorption capacity of Cu/F-rGA was 17.86 mg g^{-1}, while the adsorption capacities of GO, rGA, F-rGA, and Cu-rGA were 1.51, 3.76, 6.24, and 13.72 mg g^{-1}, respectively. The adsorption capacity of PFOA on Cu/F-rGA was increased about 4.75-fold in comparison with rGA. Compared with

https://dx.doi.org/10.1021/acsomega.1c00044
ACS Omega 2021, 6, 7073−7085

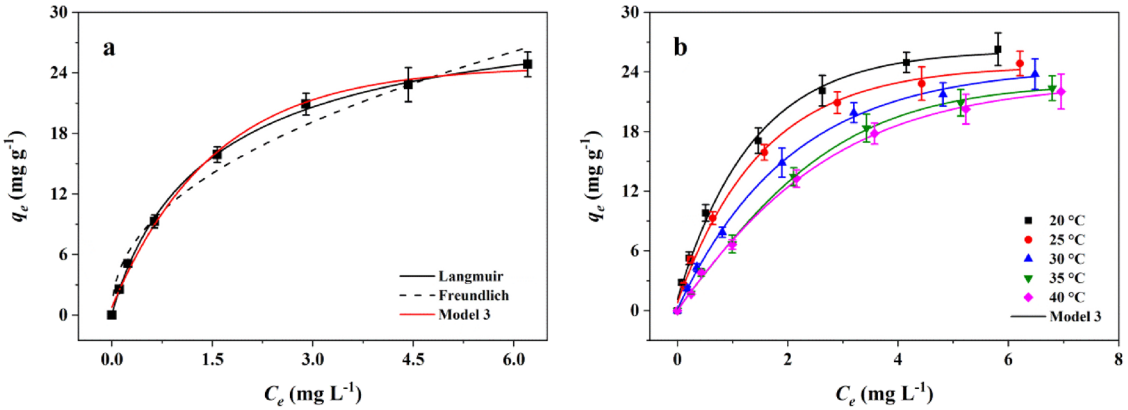

Figure 4. Adsorption isotherm data were fitted by (a) Langmuir, Freundlich, and model 3 obtained at 25 °C and (b) model 3 at different temperatures.

boehmite, graphene oxide, and lanthanum-modified graphene oxide, Cu/F-rGA had higher adsorption capacity.[45,46] This may be attributed to the large surface area, F−F interaction, and complex reaction of Cu/F-rGA.

As we know, the specific surface area was a very important factor for affecting the adsorption.[24] The adsorbents used in this study had different SSAs, which had different effects on the adsorption results. In order to eliminate the difference of adsorption capacity caused by the SSA, the adsorption capacity of these adsorbents was standardized by the SSA (Figure 3b). The adsorption capacity and adsorption trend of PFOA on these adsorbents did not significantly change. This indicated that the SSA was not the only key factor to affect the adsorption process. Some other factors also played an irreplaceable role in the adsorption.

The F−F interaction was formed with CF_2 and CF_3 of PFOA after the F element doped on GO, which improved the adsorption capacity of Cu/F-rGA.[47] In addition, after loading Cu NPs onto aerogels, PFOA formed spherical complexes through complexation to enhance its adsorption capacity.[31] It should be noted that after the adsorption process, Cu ions were detected in the supernatant and its content occupied only 0.47% of the total content of Cu NPs in Cu/F-rGA, but no F ions were detected. Cu ions can form bridges between Cu/F-rGA and PFOA, which promoted the adsorption capacity of Cu/F-rGA.[31]

Some theoretical models were also used to analyze the adsorption of PFOA on Cu/F-rGA. At present, the most frequently used models were the traditional classical adsorption models, Langmuir and Freundlich (Eqs S5 and S6, respectively).[48,49] As it is known, the two models assumed that the adsorption of the adsorbate was only carried out by forming uniform adsorption layer(s), without considering the influence of the properties of the adsorbent and the adsorbate on the adsorption. The statistical physics model comprehensively considers the influence of a variety of external factors on the adsorption, which made the fitting result more close to the actual process. Therefore, the statistical physics models (models 1−3) were selected to analyze the adsorption isotherm of Cu/F-rGA (Figure 4). By comparing R^2 and RMSE calculated in Table S4, it was determined that model 3 had an ideal fitting effect on adsorption isotherm results. At the same time, the fitting parameters of model 3 are listed in Table S5.

The captured number (n) of PFOA molecules on Cu/F-rGA was different at different temperatures. For instance, the n value was 1.32 at 35 °C, which indicated that one or two PFOA molecules were attached to an adsorption site at this temperature. ξ and $1 - \xi$ represent the percentage of one and two PFOA molecules, respectively, that is, $1 \times \xi + 2 \times (1 - \xi) = 1.32$. Therefore, 68% of the adsorption sites were anchored by one PFOA molecule, and 32% was anchored by two PFOA molecules. When $n < 1$ (20−30 °C), one PFOA molecule occupied multiple adsorption sites. In addition, the change in the value of n indicated that the orientation of adsorbed PFOA on Cu/F-rGA was angularly changed.[50] It tended to be parallel to the adsorption site at low temperature and perpendicular at high temperature.[51] The similar results were also obtained by the research of Deng et al.[24]

The density of receptor sites on Cu/F-rGA dropped from 25.51 to 12.54 mg g^{-1} (Table S5) with the increase in temperature from 20 to 40 °C. As the temperature increased, the amount of PFOA anchored to the adsorption sites of Cu/F-rGA increased. This limited the accessible free adsorption space of Cu/F-rGA, which resulted in a decrease in N_M with increasing temperature.

With the increase in temperature, the total adsorption layers ($N_C = 1 + N_2$) formed on the Cu/F-rGA surface decreased from 2.51 to 1.63. On the one hand, the temperature increase weakened the stability of the Cu/F-rGA electrical double layer and reduced the adsorption capacity of PFOA molecules in the outer layer.[52] On the other hand, the increase in temperature weakened the hydrophobicity of PFOA molecules and at the same time strengthened the thermal vibration of PFOA molecules. Finally, this reduced the adsorption layer formed by PFOA molecules on Cu/F-rGA.[53,54]

2.2.3. Adsorption−Desorption and Recycling of Cu/F-rGA. By studying the adsorption kinetics and isotherm of PFOA on aerogels, it could be known that Cu/F-rGA had the best removal effect. Therefore, the desorption behavior of Cu/F-rGA was subsequently explored, and several different electrolyte solutions were used as desorption solvents. The adsorption−desorption results are shown in Figure S4a−c. With the increase in the desorption cycles, the adsorption amount of PFOA on Cu/F-rGA gradually decreased. After the fifth desorption process, the desorption rates were 32.42, 52.31, and 74.46% with 1 mM Na_2SO_4, 100 mM Na_2SO_4, and ethanol, respectively. With the increase in ionic strength, more SO_4^{2-} formed competitive adsorption with PFOA, which led to

https://dx.doi.org/10.1021/acsomega.1c00044
ACS Omega 2021, 6, 7073−7085

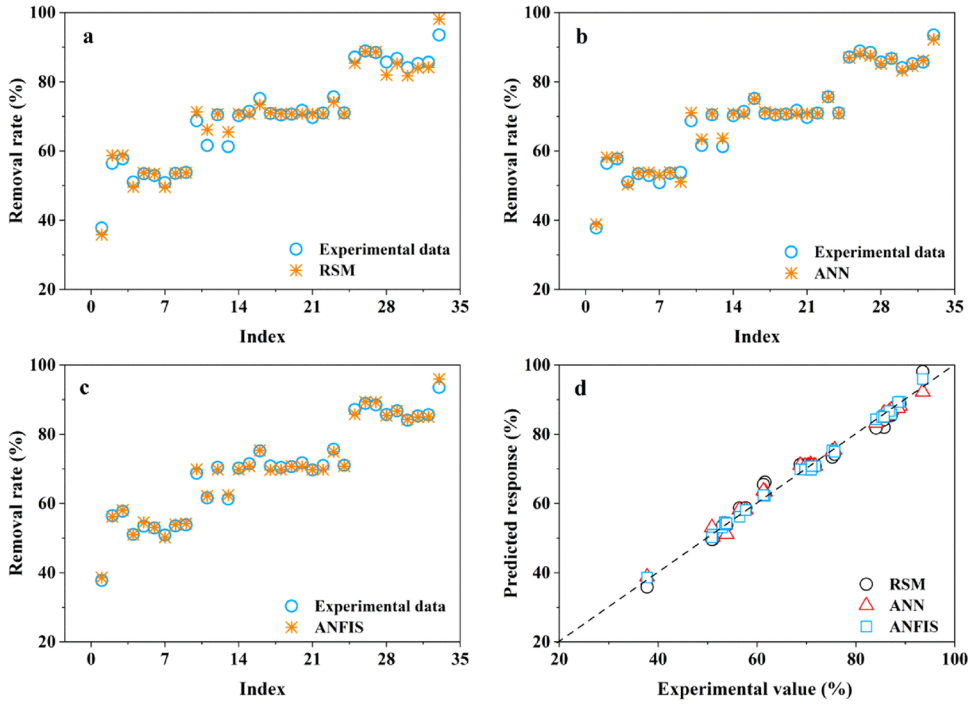

Figure 5. Removal rate of PFOA on Cu/F-rGA. The experimental values were compared with the predicted response values of (a) RSM, (b) ANN, and (c) ANFIS. (d) Comparison of predicted response values of the RSM, ANN, and ANFIS.

the desorption of PFOA into the solution. Ethanol was an organic solvent with higher solubility of PFOA than water, which led to the desorption of adsorbed PFOA into ethanol.[55] Compared with high ionic strength, ethanol was more decisive for the desorption of PFOA.

The regeneration and reusability of Cu/F-rGA were determined through multiple adsorption−desorption processes (Figure S4d). The results showed that after 10 times adsorption−desorption, the adsorption capacity of PFOA on Cu/F-rGA still maintained 73.26% of its initial capacity. Compared with the initial removal ratio of 79.58% (the 0 cycle in Figure S4d), the removal ratios of PFOA on Cu/F-rGA decreased after 10 times desorption, and the removal ratios were stable at 57.50−64.04%. This indicated that the removal ratio of Cu/F-rGA had no significant change after multiple desorption. The PFOA desorbed into the electrolyte was absorbed by the Cu/F-rGA through the physical adsorption such as the F−F interaction and hydrophobic interaction. The doping of F elements improved the apparent removal ratio of Cu/F-rGA through the F−F interaction.[37] Meanwhile, the PFOA molecules adsorbed by the chemical adsorption such as the complexation reaction between Cu NPs and PFOA were finally fixed on the Cu/F-rGA and little PFOA molecules were desorbed into the solution.[56] So, Cu/F-rGA could effectively remove PFOA from water by using ethanol and possessed excellent potential of regeneration and reuse.

2.3. Simulation. As a traditional research method, the control variable method is not only time-consuming and tedious but also does not completely describe the comprehensive effect of each variable in the adsorption process. This may lead to misinterpretation in the analysis of the results. In order to overcome these shortcomings, some statistical methods, such as the response surface method (RSM), artificial neural networks (ANNs), and adaptive neuro-fuzzy inference system (ANFIS), were used in the analysis. The RSM is useful for analyzing the effects of several independent variables.[57] It can assess the relationships between the response(s) and the independent variables. The ANN has reliable and salient characteristics in capturing the nonlinear relationships existing between variables.[57] The ANFIS can mix the learning effect of the ANN and the reasoning effect of the FIS, to result in a more realistic result.[58] Therefore, the three different methods were used to simulate the effect of variable factor (adsorbent dosage, pH, ionic strength, and temperature) on the removal rate of PFOA.

2.3.1. Analysis of CCD and RSM. Table 3 lists the design matrix of variable factors and corresponding results, including experimental values and predicted response values. The results were evaluated and analyzed by ANOVA (Table 4) using Design-Expert 11, and the approximate function (eq 1) between the variable factor and PFOA removal rate was obtained. The predicted response values corresponding to the variable factors are shown in Figure 5a. According to ANOVA analysis, the r^2 value of the model function was 0.9811, and adjusted r^2 was 0.9663, which indicated that the model accurately predicted the removal rate of PFOA.[59] In addition, the *F*-value of the model was 27.6902 and *p*-value was <0.0001, which proved that the model had statistical significance and was suitable for simulating the adsorption process of PFOA on Cu/F-rGA.

$$y = 31.63188 + 10.01542x_1 - 0.86833x_2 - 0.14881x_3 - 0.23150x_4 - 0.23430{x_1}^2 - 0.05664{x_2}^2 - 0.00006{x_3}^2 + 0.00414{x_4}^2 + 0.03859x_1x_2 + 0.01055x_1x_3 - 0.0024x_1x_4 + 0.00730x_2x_3 - 0.00219x_2x_4 \quad (1)$$

The corresponding response surface is generated in Figure S5. The response surface also proved that the dosage of Cu/F-

https://dx.doi.org/10.1021/acsomega.1c00044
ACS Omega 2021, 6, 7073−7085

Table 1. Error Rates of the RSM, ANN, and ANFIS Prediction Models

	RSM		ANN		ANFIS	
parameters	training	checking	training	checking	training	checking
R^2	0.9811	0.8933	0.9989	0.9943	0.9995	0.9966
MSE	0.4094	3.5344	0.1954	1.2258	0.0992	0.6291
SSE	0.6398	1.8800	0.4421	1.1072	0.3150	0.7931
ARE	0.4128	2.0028	0.2835	1.3428	0.1952	0.9161

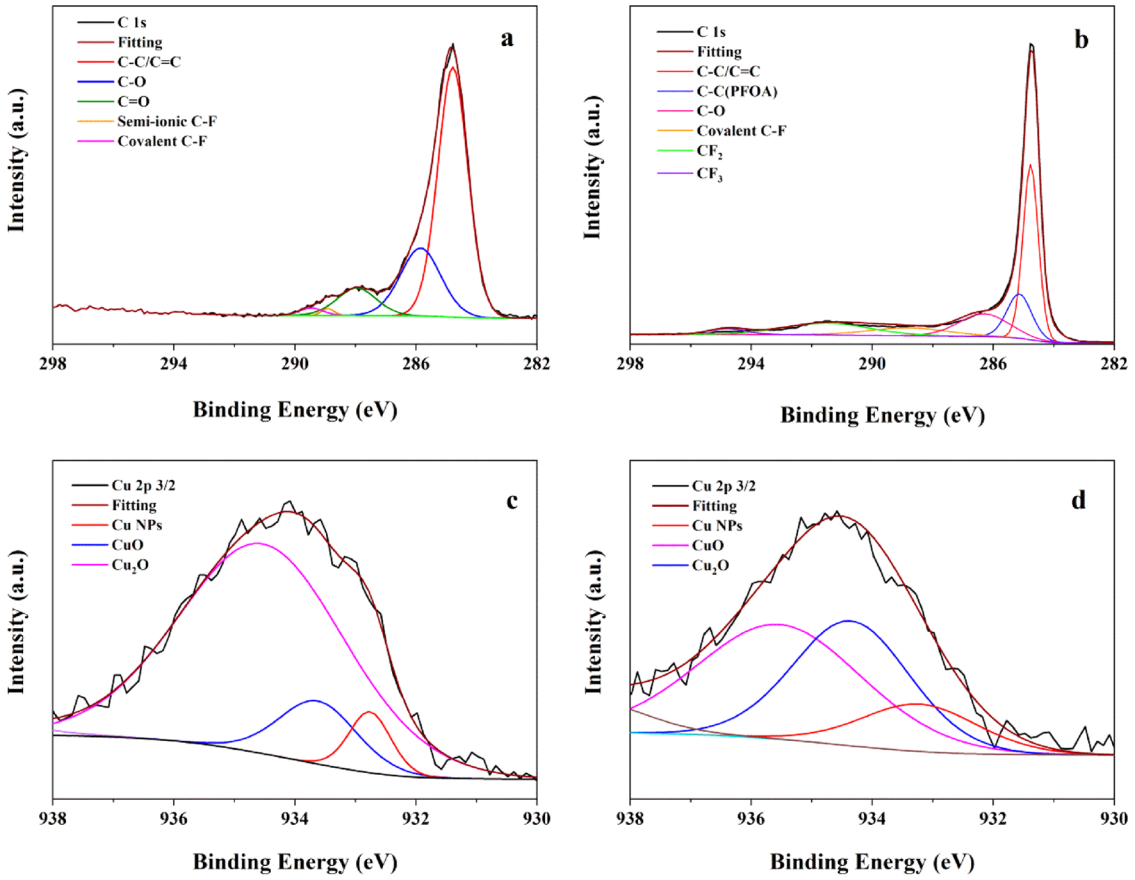

Figure 6. XPS (a, b) C 1s and (c, d) Cu $2p_{3/2}$ spectra of Cu/F-rGA before and after PFOA adsorption, respectively.

rGA had a significant effect on the removal rate of PFOA, and the pH value of the solution had a second effect on it. The ionic strength and temperature within the selected range had little effect. As the dosage of Cu/F-rGA increased, the number of available effective adsorption sites increased accordingly, thereby improving the removal rate of PFOA. The increase in the pH value caused the surface of the adsorbent to appear electronegative, which increased the electrostatic repulsion of PFOA anions, and this reduced the adsorption capacity of PFOA on Cu/F-rGA.

2.3.2. Analysis of ANN. In this study, the most suitable ANN topology included four input layers, a hidden layer with 10 neurons, and an output layer. Among them, the number of neurons in the hidden layer was considered by training various ANN topologies and selecting the best topology based on the smallest epochs and MSE.[60] As shown in Figure S6, when the hidden layer contains 10 neurons, the epoch and MSE were the smallest. Therefore, an ANN with a 4-1-1 topology was selected to determine the correlation between the PFOA removal rate and variable factors. Figure S7 shows the training, test, and validation results under the ANN topology, and r^2 was higher than 0.99. Figure 5b,d shows that the predicted response values obtained under the ANN topology were highly consistent with the experimental values, indicating that the ANN could be used to predict the removal rate of PFOA on Cu/F-rGA under a specific adsorbent dosage, pH, ionic strength, and temperature.

2.3.3. Analysis of ANFIS. The ANFIS architecture was selected by evaluating the minimum MSE for verification and running time (Figure S8).[58] The results showed that when the ANFIS contained three membership functions for adsorbent dosage, three for pH, two for ionic strength, and two for temperature, 36 multiple rules can be generated. The ANFIS in this case had the most ideal topological structure for predicting the adsorption of PFOA on Cu/F-rGA (Figure 5c,d). Figure S9 shows the three-dimensional prediction graph between the removal rate of PFOA and different variable factors. The increase in the adsorbent dosage can significantly increase the removal rate of PFOA; however, the increase in pH, ionic strength, and temperature would inhibit the removal rate. From this perspective, the predicted response values of the ANFIS were consistent with experimental values.

https://dx.doi.org/10.1021/acsomega.1c00044
ACS Omega 2021, 6, 7073−7085

2.3.4. Comparison of RSM, ANN, and ANFIS. The RSM, ANN, and ANFIS were excellent models that could solve linear and nonlinear multivariate variables. The three models were used to predict the removal rate of PFOA on Cu/F-rGA under given conditions, and the predicted response values were very suitable for experimental values (Figure 5d). Unlike the ANN and ANFIS, the RSM had a regression equation for predicting and realizing optimal conditions for variables.[59] However, the main limitation of the RSM was that it can only solve the correlation of second-order nonlinearity. In contrast, ANN and ANFIS models could solve any form of nonlinearity.[60] Table 1 lists R^2, MSE, SSE, and ARE of the RSM, ANN, and ANFIS. It indicated that compared with the RSM and ANN, the ANFIS had better accuracy and predictability in predicting the removal rate of PFOA on Cu/F-rGA. Therefore, the ANFIS could effectively evaluate and predict the removal rate of PFOA on Cu/F-rGA from aqueous solution.

2.3.5. Influence of Environmental Factors on Adsorption. As the dosage of Cu/F-rGA increased, it could provide more effective and available adsorption sites, which effectively improved the removal rate of PFOA. According to the zeta potential under different pH values in Figure S3, the zero potential point (pH_{pzc}) of Cu/F-rGA was about pH 6.3. When the equilibrium pH of the solution was less than pH_{pzc}, Cu/F-rGA exhibited electropositivity, which can improve the adsorption capacity of Cu/F-rGA for PFOA anions through electrostatic attraction; when the equilibrium pH of the solution was greater than pH_{pzc}, Cu/F-rGA exhibited electronegativity, and the Cu/F-rGA surface carried large number of positive charges and formed electrostatic repulsion with PFOA anions, which inhibited the adsorption of PFOA. The concentration of SO_4^{2-} was increased with the increase in ionic strength. So, the SO_4^{2-} and PFOA anions formed competitive adsorption and thereby weakened the adsorption capacity of PFOA on Cu/F-rGA.[61] In addition, the increase in Na^+ concentration can compress the electric double layer of Cu/F-rGA, which would reduce the removal rate of PFOA by Cu/F-rGA.[62]

2.4. Mechanisms of Adsorption. Cu/F-rGA was characterized by FTIR and XPS before and after adsorption to explore its combination with PFOA. After the adsorption, two new peaks appeared near 1149 and 1208 cm^{-1}, respectively, which were speculated to be the vibration of CF_2 and CF_3, respectively (Figure 1d and Figure S3b).[40] However, at this time, the position of the peaks was slightly shifted from the CF_2 and CF_3 characteristic peaks inherent in PFOA (1148 and 1205 cm^{-1}, respectively). This was due to the ligand exchange reaction between PFOA and Cu NPs and the F−F interaction between PFOA and doped F atoms.

As shown in Figure 6a,b, the characteristic peaks of CF_2 and CF_3 belonging to PFOA in C 1s spectra appeared at 291.5 and 294.6 eV, respectively, after the adsorption. This indicated that PFOA was adsorbed on the Cu/F-rGA. In addition, the Cu $2p_{3/2}$ spectrum slightly shifted to the high binding energy after adsorption, indicating the complexation reaction between Cu NPs and the PFOA anion (Figure 6c,d). In addition, the intensity of the Cu−O−R peak in the O 1s spectrum increased obviously (Figure S10), which indicated that the complexation exchange occurred between Cu−OH and the carboxyl group of PFOA in the adsorption.

Because the C−F chain of PFOA had strong hydrophobicity, micelles or semimicelle aggregates of PFOA were easily formed in water.[63] In addition, the unmodified regions on Cu/F-rGA were also quite hydrophobic. Therefore, the hydrophobic interaction easily occurred in this area, which promoted PFOA adsorbed on Cu/F-rGA. The free PFOA in the solution and PFOA adsorbed on the Cu/F-rGA surface were also adsorbed through the hydrophobic interaction. Meng et al. proved the key role of the hydrophobic interaction in the adsorption of PFOA.[64]

It was worth mentioning that the doping of the F element in graphene had a positive effect on the adsorption of PFOA. The doped F elements and the F atoms in the PFOA molecule form an F−F interaction, thereby improving the adsorption capacity of PFOA on Cu/F-rGA.[37] In addition, by comparing the adsorption capacity of PFOA on F-rGA and rGA (Figure 2a), it also reflected the contribution of the F−F interaction.

In addition, hydrogen bonds also participate in the adsorption of the PFOA anion on Cu/F-rGA. There were abundant hydroxyl groups on the surface of Cu NPs, which formed a complexation structure with water molecules.[65] The carboxyl and CF_3 groups of the PFOA anion formed a hydrogen bond with complex water molecules.[65,66] Beyond that, the oxygen-containing functional groups on the Cu/F-rGA could adsorb PFOA through negative charge-assisted hydrogen bonding.[67]

3. CONCLUSIONS

In this work, Cu/F-rGA was prepared by the microbubble template method. Through a series of characterizations, such as SEM, EDS, FTIR, XRD, and XPS, it was proved that the F element was doped and Cu NPs were loaded on Cu/F-rGA. The adsorption kinetics showed that the adsorption of PFOA on Cu/F-rGA reached equilibrium within 360 min, and the internal diffusion process was the main rate-limiting step. The adsorption process involved physical and chemical adsorption. The adsorption isotherm indicated that F doping and Cu NP loading significantly increased the adsorption capacity of PFOA on Cu/F-rGA. The adsorption isotherm from 20 to 40 °C showed that the density of receptor sites and the number of adsorption layers of PFOA on Cu/F-rGA decreased with the increase in temperature in the medium. The hydrophobic interaction, ligand exchange reaction, F−F interaction, and hydrogen bonding play important roles in the adsorption. Ethanol can effectively regenerate Cu/F-rGA. Three models of the RSM, ANN, and ANFIS were used to fit the predicted response values of the removal rate of PFOA on Cu/F-rGA under different variable factors. Compared with the RSM and ANN, the ANFIS model had more accurate analysis and prediction response values. These provided a theoretical basis and microscopic explanation for the adsorption of PFOA on Cu/F-rGA.

4. EXPERIMENTAL SECTION

4.1. Materials. Graphite powder (325 mesh) was purchased from Qingdao Nanshu Ruiying Graphite Co., Ltd. (Qingdao, China). PFOA (96% purity) was purchased from KMF Laborchemie Handels GmbH (Germany). Other chemicals and reagents (including acetonitrile, methanol, ethanol, Na_2SO_4, etc.) used in the experiments were of analytical grade or higher. PFOA stock solution was prepared by dissolving in methanol and stored at 4 °C. In order to reduce the cosolvent effect, the volume ratio of methanol in aqueous solution of all adsorption systems was controlled below 0.1%.

https://dx.doi.org/10.1021/acsomega.1c00044
ACS Omega 2021, 6, 7073−7085

Table 2. Independent Variables and Their Levels Used in the Central Composite Design

variables	unit	factor code	levels of factors				
			lowest ($-\alpha$)	low (-1)	central (0)	high ($+1$)	highest ($+\alpha$)
adsorbent dosage	mg	x_1	2	4	6	8	10
pH		x_2	2	4	6	8	10
ionic strength	mM	x_3	0	20	40	60	80
temperature	°C	x_4	20	25	30	35	40

Table 3. Experimental Design Matrix with Observed and Predicted Values Using RSM, ANN, and ANFIS Models

run	factors				experimental value (%)	predicted response value (%)		
	x_1	x_2	x_3	x_4		RSM	ANN	ANFIS
1	2	6	40	30	37.77	35.87	38.81	38.57
2	4	4	20	35	56.45	58.73	58.20	56.17
3	4	4	20	25	57.73	58.74	58.20	58.07
4	4	8	60	25	51.08	49.65	50.35	51.00
5	4	4	60	35	53.46	53.70	53.78	54.56
6	4	8	20	35	52.95	53.43	53.83	53.11
7	4	8	60	35	50.87	49.57	53.05	50.20
8	4	8	20	25	53.56	53.53	53.87	53.91
9	4	4	60	25	53.85	53.69	51.10	54.26
10	6	6	40	20	68.76	71.27	71.08	69.90
11	6	6	80	30	61.61	66.16	63.37	62.19
12	6	6	40	30	70.46	70.76	70.80	69.80
13	6	10	40	30	61.31	65.49	63.66	62.44
14	6	6	40	30	70.23	70.76	70.80	69.80
15	6	6	40	30	71.49	70.76	70.80	70.80
16	6	6	0	30	75.21	73.38	75.06	75.41
17	6	6	40	40	70.86	71.07	71.28	69.71
18	6	6	40	30	70.43	70.76	70.80	69.80
19	6	6	40	30	70.67	70.76	70.80	70.80
20	6	6	40	30	71.78	70.76	70.80	70.80
21	6	6	40	30	69.72	70.76	70.80	69.80
22	6	6	40	30	70.98	70.76	70.80	69.80
23	6	2	40	30	75.68	74.21	75.55	74.96
24	6	6	40	30	71.06	70.76	70.80	70.80
25	8	4	60	25	87.16	85.42	87.00	85.80
26	8	4	20	25	88.92	88.77	88.15	89.41
27	8	4	20	35	88.50	88.66	87.54	89.31
28	8	8	60	25	85.72	81.99	85.22	85.44
29	8	4	60	35	86.74	85.32	86.63	86.70
30	8	8	60	35	84.08	81.81	83.29	84.34
31	8	8	20	35	85.28	83.98	84.63	84.95
32	8	8	20	25	85.68	84.18	86.13	85.05
33	10	6	40	30	93.53	98.14	92.24	95.94

4.2. Fabrication of F-rGA. GO was prepared from graphite according to a modified Hummer's method (Supporting Information).[68] In order to obtain F-rGA, fluorinated GO (F-GO) was first prepared (Supporting Information).[40] In a typical fabrication process, 50 mg of F-GO and 50 mg of sodium dodecyl sulfate (SDS) were dispersed in 10 and 1 mL of deionized water, respectively, and mixed evenly. Then, 100 mg of L-ascorbic acid (L-AA) was added into the mixed solution. The template foams were formed after stirring the mixed solution at 2500 rpm for 10 min. Then, the template foam was sealed and heated at 80 °C for 12 h to obtain hydrogel. The hydrogel was frozen at −18 °C for 4 h and then thawed at 25 °C. The hydrogel was washed several times with ethanol to remove unreacted substances. F-rGA could be obtained by drying the hydrogel at room temperature.

4.3. Fabrication of Cu/F-rGA. First, 16 mg of poly(vinylpyrrolidone) (PVP) and 80 mg of $CuSO_4 \cdot 5H_2O$ were dissolved into 50 mL of deionized water. Then, 5 mg of F-rGA was soaked in the above mixed solution at 25 °C for 24 h and was dried in a vacuum drying oven. Finally, the sample was pyrolyzed at 500 °C for 2 h under the protection of Ar, and Cu/F-rGA aerogel can be obtained after cooling to room temperature.

In addition, reduced graphene oxide aerogel (rGA) and Cu NP-loaded rGA (Cu-rGA) were also prepared as control groups (Supporting Information).

4.4. Characterization. The specific surface areas (SSAs) of aerogels determined by nitrogen adsorption−desorption isotherms were measured using a surface area analyzer (NOVA 1200e, Quantachrome, America) through the multi-point Brunauer−Emmett−Teller (BET) method, and the pore

https://dx.doi.org/10.1021/acsomega.1c00044
ACS Omega 2021, 6, 7073−7085

size distribution was based on the nonlocal density functional theory (NL-DFT) model. The zeta potentials of aerogels were determined using a laser particle size analyzer (Zetasizer Nano S, Malvern, UK). Microscopy images were observed by scanning electron microscopy (SEM, SU8020, Hitachi, Japan). X-ray diffraction (XRD, Rigaku D/max 2550, Shimadzu, Japan) with Cu Kα radiation was used to identify the phase composition. The surface functional groups were ensured by X-ray photoelectron spectroscopy (XPS, Thermo ESCALAB 250Xi, America) and Fourier transform infrared spectroscopy (FTIR, Thermo Fisher, America). XPS spectra were analyzed by Thermo Avantage software. FTIR spectra were recorded on the spectrum in the 4000−400 cm^{-1} region with a resolution of 2 cm^{-1} in transmission mode. ICP-OES (iCAP 7000, Thermo Fisher, America) was used to determine the concentrations of Cu and F ions in solution.

4.5. Adsorption Experiments. All adsorption experiments were performed by a batch equilibration technique, and each treatment was executed in three replications. The adsorption kinetics of adsorbents were carried out using 10 mg L^{-1} PFOA. Adsorbents (6 mg) were weighted into 40 mL of aqueous solution (pH 6.00 ± 0.10) containing 1 mM Na_2SO_4 and prewetted for 24 h. Then, the adsorption capacity of adsorbent was measured at the set time point. The whole process was carried out under shading conditions.

For adsorption isotherms, different initial PFOA concentrations (0.5−10 mg L^{-1}) were used to determine the adsorption isotherms of adsorbents. According to the adsorption kinetic results, 12 h was selected as the adsorption time, and then the supernatant was taken out to determine the concentration of PFOA. After reaching the adsorption equilibrium, 5.0 mL of supernatant was taken out and filtered, and then it was used to detect the concentration of PFOA. Other conditions were the same as adsorption kinetics. Ultraperformance liquid chromatography (UPLC) was used to quantify the concentration of PFOA, and the specific analysis method was described in the Supporting Information. The pH value of electrolyte solution was adjusted to 6.07 before adsorption and changed to 5.92 after adsorption. The ionic strength was measured using a Na^+ electrode, and there was no significant change before and after adsorption.

In order to study the regeneration of Cu/F-rGA, 1 and 100 mM Na_2SO_4 and ethanol were selected as the desorption solvent. After adsorption equilibrium, 50% volume of solution was displaced by the desorption solvent. Other conditions were the same as the adsorption process. This operation was carried out five times.

4.6. Simulation Analysis. *4.6.1. Response Surface Methodology (RSM).* In order to explore the common influence of different environmental factors on the adsorption of PFOA on Cu/F-rGA, the RSM was used to optimize and analyze the relationship between variables and responses. Central composite design (CCD, Design-Expert 11, Stat-Ease, Inc.) was selected to design the combination of different environmental factors. In this work, four important factors, namely, adsorbent dosage (x_1), solution pH (x_2), ionic strength (x_3), and temperature (x_4), were considered. Table 2 shows the actual and coded values of these four factors. Each variable was coded as high (+1) and low (−1), while the axis points were coded as $+\alpha$ and $-\alpha$. In order to make the design between various factors more stable, 9 points were selected and 33 groups of experiments were carried out. The corresponding combination design and test results are listed in Table 3. The correlation between environmental factors and responses was expressed as the following quadratic equation

$$y = b_0 + \sum_{i=1}^{N} b_i x_i + \sum_{i=1}^{N} b_i x_i^2 + \sum_{i=1,j=1}^{N} b_{ij} x_i x_j + \varepsilon \quad (2)$$

where y is the predicted response (predicted removal rate, R %); x_i and x_j are the independent variables in coded levels; and b_i, b_{ii}, b_{ij} are the coefficient for linear, quadratic, and interaction effect, respectively. b_0 and ε are the model coefficient and error, respectively. N is the number of factors (independent variables). The analysis of variance (ANOVA) was applied to estimate the significance of the independent parameters and their interactions.

Table 4. ANOVA for the Response Surface Quadratic Model

source of variation	sum of squares	degree of freedom	mean square	F-value	p-value
model	6043.4721	14	431.6766	66.6194	<0.0001
x_1	5816.9521	1	5816.9521	897.7140	<0.0001
x_2	114.1012	1	114.1012	17.6089	0.0005
x_3	78.1926	1	78.1926	12.0672	0.0027
x_4	0.0570	1	0.0570	0.0088	0.9263
x_1x_2	0.3813	1	0.3813	0.0588	0.8111
x_1x_3	2.8477	1	2.8477	0.4395	0.5158
x_1x_4	0.0095	1	0.0095	0.0015	0.9699
x_2x_3	1.3631	1	1.3631	0.2104	0.6520
x_2x_4	0.0077	1	0.0077	0.0012	0.9730
x_3x_4	0.0002	1	0.0002	0.0000	0.9961
x_1^2	26.6270	1	26.6270	4.1093	0.0577
x_2^2	1.5561	1	1.5561	0.2402	0.6300
x_3^2	1.8523	1	1.8523	0.2859	0.5994
x_4^2	0.3244	1	0.3244	0.0501	0.8255
residual	116.6353	18	6.4797		
lack of fit	113.3602	10	11.3360	27.6902	<0.0001
pure error	3.2751	8	0.4094		
cor. total	6160.1074	32			

4.6.2. Artificial Neural Network (ANN). In this study, the ANN was selected to apply for the nonparametric modeling and the optimization. This process was carried out using the MATLAB neural network toolboxes, and the removal efficiency of PFOA in aqueous solution was predicted. One input layer, one hidden layer, and one output layer were set in the selected ANN (Figure S11). The input layer neurons include four variables, i.e., the adsorbent dosage, solution pH, ionic strength, and temperature. The output layer had one neuron, namely, removal efficiency. The Levenberg−Marquardt back propagation algorithm was selected to train the network. The input−output data were divided into three subsets, of which 70% was used for training, 15% for testing, and 15% for verification. The same other parameters of the ANN are shown in Table S6.

4.6.3. Adaptive Neuro-Fuzzy Inference System (ANFIS). The ANFIS is an inference system formed by the combination of the fuzzy inference system (FIS) and ANN. It can effectively solve nonlinear and complex problems within a framework. The ANFIS is also analyzed using the toolbox embedded in MATLAB, and the removal efficiency of PFOA in aqueous solution was predicted. In this study, the ANFIS structure was built in four layers (Figure S12), that is, the input layer (the adsorbent dosage, solution pH, ionic strength, and temper-

https://dx.doi.org/10.1021/acsomega.1c00044
ACS Omega 2021, 6, 7073−7085

ature), the inference layer with weight rules, the defuzzification layer, and the output layer (removal efficiency). The parameters of the ANFIS are shown in Table S7.

The performance of the RSM, ANN, and ANFIS models was evaluated by the sum of squared errors (SSE), mean squared error (MSE), average relative error (ARE), and coefficient of determination (R^2), which were calculated using the following equations[69,70]

$$\mathrm{SSE} = \sqrt{\frac{\sum_{i=1}^{N} (y_{i,\mathrm{exp}} - y_{i,\mathrm{pred}})^2}{N}} \quad (3)$$

$$\mathrm{MSE} = \frac{1}{N}\sum_{i=1}^{N} (y_{i,\mathrm{pred}} - y_{i,\mathrm{exp}})^2 \quad (4)$$

$$\mathrm{ARE} = \frac{100}{N}\sum_{i=1}^{N} \left| \frac{y_{i,\mathrm{pred}} - y_{i,\mathrm{exp}}}{y_{i,\mathrm{exp}}} \right| \% \quad (5)$$

$$R^2 = 1 - \sum_{i=1}^{N} \left(\frac{(y_{i,\mathrm{pred}} - y_{i,\mathrm{exp}})^2}{(y_{\mathrm{avg,exp}} - y_{i,\mathrm{exp}})^2} \right) \quad (6)$$

where N is the number of experimental data and $y_{i,\mathrm{pred}}$ and $y_{i,\mathrm{exp}}$ are the predicted and experimental values, respectively. $y_{\mathrm{avg,exp}}$ is the average of experimental values.

The removal rate (%) of PFOA was calculated using the following equation

$$R(\%) = \frac{(C_0 - C_e)}{C_0} \times 100 \quad (7)$$

where C_0 (mg L^{-1}) is the initial PFOA concentration and C_e (mg L^{-1}) is the equilibrium concentration.

4.7. Data Analysis. Specific information about the mathematical models simulated adsorption kinetic and isotherm data is shown in the Supporting Information. Pseudo-first-order, pseudo-second-order, intraparticle diffusion, and Boyd models were used to fit adsorption kinetic data, and Langmuir, Freundlich, and three statistical physics models (models 1−3)[71,72] were used to fit adsorption isotherm data, respectively. The models were analyzed using Origin 2019. In addition, bars in the figures represent standard errors.

4.7.1. Model 1: Statistical Physics Model with One Layer of Adsorbed PFOA Molecules. This model assumed that there was only one adsorption layer between PFOA molecules and Cu/F-rGA but could capture a variable number of PFOA molecules, which was different to the fundaments of the Langmuir model. The expression of the model was given by the following expression

$$q_e = \frac{n \cdot N_M}{1 + \left(\frac{C_{1/2}}{C_e}\right)^n}$$

where the parameter n represents the captured number of PFOA molecules per adsorption site, N_M (mg g^{-1}) is the density of receptor sites of Cu/F-rGA, and $C_{1/2}$ (mg L^{-1}) is the concentration at half-saturation.

4.7.2. Model 2: Statistical Physics Model with Two Layers of adsorbed PFOA Molecules. This model assumed that PFOA adsorption on Cu/F-rGA occurred by a formation of two adsorbed layers. The first layer was PFOA molecules anchored on the adsorption site, and the second one involved the anchored PFOA molecules and free PFOA molecules. The expression of the model was given by the following expression

$$q_e = n \cdot N_M \frac{\left(\frac{C_e}{C_1}\right)^n + 2\left(\frac{C_e}{C_2}\right)^{2n}}{1 + \left(\frac{C_e}{C_1}\right)^n + \left(\frac{C_e}{C_2}\right)^{2n}}$$

where C_1 (mg L^{-1}) and C_2 (mg L^{-1}) are defined as concentrations at half-saturation that were related to first and second adsorbed layers of the PFOA molecules, respectively.

4.7.3. Model 3: Statistical Physics Model with a Variable Number of Layers of Adsorbed PFOA Molecules. This model assumed that PFOA adsorption on Cu/F-rGA was performed via a variable number of layers (1 + N_2). The number 1 represents the first adsorbed layer that PFOA molecules anchored on the adsorption site, and N_2 represents a variable number of layers formed by free PFOA molecules. The expression of the model was given by the following expression

$$q_e = n \cdot N_M \frac{\frac{-2\left(\frac{C_e}{C_1}\right)^{2n}}{1-\left(\frac{C_e}{C_1}\right)^n} + \frac{\left(\frac{C_e}{C_1}\right)^n\left(\frac{C_e}{C_1}\right)^{2n}}{\left(1-\left(\frac{C_e}{C_1}\right)^n\right)^2} + \frac{2\left(\frac{C_e}{C_1}\right)^n\left(\frac{C_e}{C_2}\right)^n\left(1-\left(\frac{C_e}{C_2}\right)^{nN_2}\right)}{1-\left(\frac{C_e}{C_2}\right)^n} - \frac{N_2\left(\frac{C_e}{C_1}\right)^n\left(\frac{C_e}{C_2}\right)^n\left(\frac{C_e}{C_2}\right)^{nN_2}\left(1-\left(\frac{C_e}{C_2}\right)^n\right)}{1-\left(\frac{C_e}{C_2}\right)^n} + \frac{\left(\frac{C_e}{C_1}\right)^n\left(\frac{C_e}{C_2}\right)^{2n}\left(1-\left(\frac{C_e}{C_2}\right)^{nN_2}\right)}{\left(1-\left(\frac{C_e}{C_2}\right)^n\right)^2}}{\frac{1-\left(\frac{C_e}{C_1}\right)^{2n}}{1-\left(\frac{C_e}{C_1}\right)^n} + \frac{\left(\frac{C_e}{C_1}\right)^n\left(\frac{C_e}{C_2}\right)^n\left(1-\left(\frac{C_e}{C_2}\right)^{nN_2}\right)}{1-\left(\frac{C_e}{C_2}\right)^n}}$$

where C_1 (mg L^{-1}) and C_2 (mg L^{-1}) are the concentrations at half-saturation of the first and the N_2 layers, respectively. Therefore, the total number of adsorbed dye layers is defined as $N_C = 1 + N_2$.

■ ASSOCIATED CONTENT

Supporting Information

The Supporting Information is available free of charge at https://pubs.acs.org/doi/10.1021/acsomega.1c00044.

Part I: (1) synthesis of graphene oxide (GO); (2) synthesis of fluorinated GO (F-GO); (3) synthesis of reduced graphene oxide aerogel (rGA); (4) synthesis of Cu NP-loaded rGA (Cu-rGA); (5) UPLC analytical method of PFOA; (6) adsorption kinetic models; and (7) adsorption isotherm models; part II: Figure S1, the stability of Cu/F-rGA after 48 h of equilibrium in different pH values (4.11, 7.08, and 10.06), ionic strengths (10, 50, and 100 mM), and liquid media (acetone, chloroform, and ethanol); Figure S2, characterization of Cu/F-rGA (typical SEM of Cu/F-rGA and EDS mapping images of Cu/F-rGA); Figure S3, Characterization of zeta potential of rGA, F-rGA, Cu-rGA, and Cu/F-rGA at different equilibrium pH values and FTIR spectrum of Cu/F-rGA before and after

https://dx.doi.org/10.1021/acsomega.1c00044
ACS Omega 2021, 6, 7073−7085

PFOA adsorption; Figure S4, adsorption−desorption behaviors of PFOA on Cu/F-rGA (1 mM Na_2SO_4, 100 mM Na_2SO_4, and ethanol were used as electrolyte solution in the desorption process) and removal capacity of PFOA on Cu/F-rGA within 10 times adsorption−desorption (ethanol was used as desorption solution); Figure S5, response surface of the RSM for the Cu/F-rGA adsorbent; Figure S6, MSE and epoch with different hidden layers; Figure S7, training, test, and validation results and performance plot (MSE) under the 4-1-1 ANN topology; Figure S8, ANFIS architecture search; Figure S9, surface output of the ANFIS model for the Cu/F-rGA adsorbent; Figure S10, XPS O 1s spectra of Cu/F-rGA before and after PFOA adsorption; Figure S11, artificial neural network architecture; and Figure S12, simplified version of the ANFIS architecture; and part III: Table S1, some typical physic-chemical properties of PFOA; Table S2, physic-chemical properties of GO and different aerogels; Table S3, adsorption kinetic parameters of PFOA on different aerogels; Table S4, RMSE and R^2 values of test models; Table S5, parameters of model 3 for the adsorption of PFOA on Cu/F-rGA; Table S6, parameters of the ANN; and Table S7, parameters of the ANFIS (PDF)

AUTHOR INFORMATION

Corresponding Authors

Yanli Liu − *National Engineering Laboratory for Efficient Utilization of Soil and Fertilizer Resources, College of Resources and Environment, Shandong Agricultural University, Tai'an 271018, China*; Phone: +86-538-824 2250; Email: yanliliu2013@163.com

Chengliang Li − *National Engineering Laboratory for Efficient Utilization of Soil and Fertilizer Resources, College of Resources and Environment, Shandong Agricultural University, Tai'an 271018, China*; orcid.org/0000-0002-8116-2372; Phone: +86-538-824 5558; Email: chengliang_li11@163.com

Authors

Longfei Liu − *National Engineering Laboratory for Efficient Utilization of Soil and Fertilizer Resources, College of Resources and Environment, Shandong Agricultural University, Tai'an 271018, China*

Naiju Che − *National Engineering Laboratory for Efficient Utilization of Soil and Fertilizer Resources, College of Resources and Environment, Shandong Agricultural University, Tai'an 271018, China*

Shengsen Wang − *College of Environmental Science and Engineering, Yangzhou University, Yangzhou 225127, China*

Complete contact information is available at: https://pubs.acs.org/10.1021/acsomega.1c00044

Author Contributions

L.L. conceptualized the study, performed the methodology part, and wrote the original draft of the manuscript. L.L. and C.L. performed data curation. L.L., N.C., S.W., and C.L. performed formal analysis. N.C., S.W., and C.L. validated and visualized the study. Y.L. and C.L. supervised the study and edited and reviewed the manuscript. N.C. analyzed the software results. Y.L. investigated and administered the project. C.L. acquired funding.

Notes

The authors declare no competing financial interest.

ACKNOWLEDGMENTS

This work was financially supported by the National Natural Science Foundation of China (project no. 21377074).

REFERENCES

(1) Buck, R. C.; Franklin, J.; Berger, U.; Conder, J. M.; Cousins, I. T.; De Voogt, P.; Jensen, A. A.; Kannan, K.; Mabury, S. A.; van Leeuwen, S. P. J. Perfluoroalkyl and polyfluoroalkyl substances in the environment: Terminology, classification, and origins. *Integr. Environ. Assess. Manage.* **2011**, *7*, 513−541.

(2) Li, R.; Munoz, G.; Liu, Y.; Sauvé, S.; Ghoshal, S.; Liu, J. Transformation of novel polyfluoroalkyl substances (PFASs) as co-contaminants during biopile remediation of petroleum hydrocarbons. *J. Hazard. Mater.* **2019**, *362*, 140−147.

(3) Liu, L.; Liu, Y.; Gao, B.; Ji, R.; Li, C.; Wang, S. Removal of perfluorooctanoic acid (PFOA) and perfluorooctane sulfonate (PFOS) from water by carbonaceous nanomaterials: A review. *Crit. Rev. Environ. Sci. Technol.* **2020**, *50*, 2379−2414.

(4) Singh, R. K.; Fernando, S.; Baygi, S. F.; Multari, N.; Thagard, S. M.; Holsen, T. M. Breakdown products from perfluorinated alkyl substances (PFAS) degradation in a plasma-based water treatment process. *Environ. Sci. Technol.* **2019**, *53*, 2731−2738.

(5) Wang, N.; Lv, H.; Zhou, Y.; Zhu, L.; Hu, Y.; Majima, T.; Tang, H. Complete defluorination and mineralization of perfluorooctanoic acid by a mechanochemical method using alumina and persulfate. *Environ. Sci. Technol.* **2019**, *53*, 8302−8313.

(6) Yin, T.; Chen, H.; Reinhard, M.; Yi, X.; He, Y.; Gin, K. Y.-H. Perfluoroalkyl and polyfluoroalkyl substances removal in a full-scale tropical constructed wetland system treating landfill leachate. *Water Res.* **2017**, *125*, 418−426.

(7) Coggan, T. L.; Anumol, T.; Pyke, J.; Shimeta, J.; Clarke, B. O. A single analytical method for the determination of 53 legacy and emerging per- and polyfluoroalkyl substances (PFAS) in aqueous matrices. *Anal. Bioanal. Chem.* **2019**, *411*, 3507−3520.

(8) Gao, K.; Fu, J.; Xue, Q.; Li, Y.; Liang, Y.; Pan, Y.; Zhang, A.; Jiang, G. An integrated method for simultaneously determining 10 classes of per- and polyfluoroalkyl substances in one drop of human serum. *Anal. Chim. Acta* **2018**, *999*, 76−86.

(9) Li, R.; Shi, Y.; Wu, M.; Hong, S.; Wang, P. Photovoltaic panel cooling by atmospheric water sorption−evaporation cycle. *Nat. Sustainability* **2020**, 636.

(10) Xiao, F.; Simcik, M. F.; Halbach, T. R.; Gulliver, J. S. Perfluorooctane sulfonate (PFOS) and perfluorooctanoate (PFOA) in soils and groundwater of a U.S. metropolitan area: migration and implications for human exposure. *Water Res.* **2015**, *72*, 64−74.

(11) Agency for Toxic Substances and Disease Registry (ATSDR) *Toxicological profile for perfluoroalkyls*; 2018, Retrieved from https://www.atsdr.cdc.gov/ToxProfiles/tp.asp?id=1117&tid=237.

(12) Agency for Toxic Substances and Disease Registry (ATSDR) *Per and polyfluoroalkyl substances (PFAS) in the pease tradeport public water system*; 2019, Retrieved from https://www.atsdr.cdc.gov/HAC/pha/pease/Pease-Tradeport-Public-Water-PFAS-HC-508.pdf.

(13) Pei, C.-Y.; Chen, Y.-G.; Wang, L.; Chen, W.; Huang, G.-B. Step-scheme $WO_3/CdIn_2S_4$ hybrid system with high visible light activity for tetracycline hydrochloride photodegradation. *Appl. Surf. Sci.* **2021**, *535*, 147682.

(14) Duan, C.; Yu, Y.; Xiao, J.; Li, Y.; Yang, P.; Hu, F.; Xi, H. Recent advancements in metal−organic frameworks for green applications. *Green Energy Environ.* **2020**, DOI: 10.1016/j.gee.2020.04.006.

(15) Duan, C.; Yu, Y.; Li, J.; Li, L.; Huang, B.; Chen, D.; Xi, H. Recent advances in the synthesis of monolithic metal−organic frameworks. *Sci. China Mater.* **2021**, DOI: 10.1007/s40843-020-1585-1.

(16) Arvaniti, O. S.; Hwang, Y.; Andersen, H. R.; Stasinakis, A. S.; Thomaidis, N. S.; Aloupi, M. Reductive degradation of perfluorinated

compounds in water using Mg-aminoclay coated nanoscale zero valent iron. *Chem. Eng. J.* **2015**, *262*, 133−139.
(17) Gomez-Ruiz, B.; Ribao, P.; Diban, N.; Rivero, M. J.; Ortiz, I.; Urtiaga, A. Photocatalytic degradation and mineralization of perfluorooctanoic acid (PFOA) using a composite TiO_2-rGO catalyst. *J. Hazard. Mater.* **2018**, *344*, 950−957.
(18) Shang, E.; Li, Y.; Niu, J.; Li, S.; Zhang, G.; Wang, X. Photocatalytic degradation of perfluorooctanoic acid over Pb-$BiFeO_3$/rGO catalyst: Kinetics and mechanism. *Chemosphere* **2018**, *211*, 34−43.
(19) Wang, Q.; Liu, M.; Zhao, H.; Chen, Y.; Xiao, F.; Chu, W.; Zhao, G. Efficiently degradation of perfluorooctanoic acid in synergic electrochemical process combining cathodic electro-Fenton and anodic oxidation. *Chem. Eng. J.* **2019**, *378*, 122071.
(20) Li, F.; Duan, J.; Tian, S.; Ji, H.; Zhu, Y.; Wei, Z.; Zhao, D. Short-chain per- and polyfluoroalkyl substances in aquatic systems: Occurrence, impacts and treatment. *Chem. Eng. J.* **2020**, *380*, 122506.
(21) Du, Z.; Deng, S.; Liu, D.; Yao, X.; Wang, Y.; Lu, X.; Wang, B.; Huang, J.; Wang, Y.; Xing, B.; Yu, G. Efficient adsorption of PFOS and F53B from chrome plating wastewater and their subsequent degradation in the regeneration process. *Chem. Eng. J.* **2016**, *290*, 405−413.
(22) Du, Z.; Deng, S.; Zhang, S.; Wang, B.; Huang, J.; Wang, Y.; Yu, G.; Xing, B. Selective and high sorption of perfluorooctanesulfonate and perfluorooctanoate by fluorinated alkyl chain modified montmorillonite. *J. Phys. Chem. C* **2016**, *120*, 16782−16790.
(23) Qu, Y.; Zhang, C.; Li, F.; Bo, X.; Liu, G.; Zhou, Q. Equilibrium and kinetics study on the adsorption of perfluorooctanoic acid from aqueous solution onto powdered activated carbon. *J. Hazard. Mater.* **2009**, *169*, 146−152.
(24) Deng, S.; Zhang, Q.; Nie, Y.; Wei, H.; Wang, B.; Huang, J.; Yu, G.; Xing, B. Sorption mechanisms of perfluorinated compounds on carbon nanotubes. *Environ. Pollut.* **2012**, *168*, 138−144.
(25) Oliver, D. P.; Navarro, D. A.; Baldock, J.; Simpson, S. L.; Kookana, R. S. Sorption behaviour of per- and polyfluoroalkyl substances (PFASs) as affected by the properties of coastal estuarine sediments. *Sci. Total Environ.* **2020**, *720*, 137263.
(26) Zhang, D.; Luo, Q.; Gao, B.; Chiang, S.-Y. D.; Woodward, D.; Huang, Q. Sorption of perfluorooctanoic acid, perfluorooctane sulfonate and perfluoroheptanoic acid on granular activated carbon. *Chemosphere* **2016**, *144*, 2336−2342.
(27) Liu, Y.; Ptacek, C. J.; Baldwin, R. J.; Cooper, J. M.; Blowes, D. W. Application of zero-valent iron coupled with biochar for removal of perfluoroalkyl carboxylic and sulfonic acids from water under ambient environmental conditions. *Sci. Total Environ.* **2020**, *719*, 137372.
(28) Hassan, M.; Liu, Y.; Naidu, R.; Du, J.; Qi, F. Adsorption of Perfluorooctane sulfonate (PFOS) onto metal oxides modified biochar. *Environ. Technol. Innovation* **2020**, *19*, 100816.
(29) Xing, D. Y.; Chen, Y.; Zhu, J.; Liu, T. Fabrication of hydrolytically stable magnetic core-shell aminosilane nanocomposite for the adsorption of PFOS and PFOA. *Chemosphere* **2020**, *251*, 126384.
(30) Zhou, Y.; He, Z.; Tao, Y.; Xiao, Y.; Zhou, T.; Jing, T.; Zhou, Y.; Mei, S. Preparation of a functional silica membrane coated on Fe_3O_4 nanoparticle for rapid and selective removal of perfluorinated compounds from surface water sample. *Chem. Eng. J.* **2016**, *303*, 156−166.
(31) Liu, L.; Li, D.; Li, C.; Ji, R.; Tian, X. Metal nanoparticles by doping carbon nanotubes improved the sorption of perfluorooctanoic acid. *J. Hazard. Mater.* **2018**, *351*, 206−214.
(32) Xu, J.; Liu, Z.; Zhao, D.; Gao, N.; Fu, X. Enhanced adsorption of perfluorooctanoic acid (PFOA) from water by granular activated carbon supported magnetite nanoparticles. *Sci. Total Environ.* **2020**, *723*, 137757.
(33) Yang, Y.; Zheng, Z.; Ji, W.; Xu, J.; Zhang, X. Insights to perfluorooctanoic acid adsorption micro-mechanism over Fe-based metal organic frameworks: Combining computational calculation with response surface methodology. *J. Hazard. Mater.* **2020**, *395*, 122686.
(34) Gorgolis, G.; Galiotis, C. Graphene aerogels: A review. *2D Mater.* **2017**, *4*, No. 032001.
(35) Xiao, J.; Zhang, J.; Lv, W.; Song, Y.; Zheng, Q. Multifunctional graphene/poly(vinyl alcohol) aerogels: In situ hydrothermal preparation and applications in broad-spectrum adsorption for dyes and oils. *Carbon* **2017**, *123*, 354−363.
(36) Liu, L.; Liu, Y.; Li, C.; Ji, R.; Tian, X. Improved sorption of perfluorooctanoic acid on carbon nanotubes hybridized by metal oxide nanoparticles. *Environ. Sci. Pollut. Res.* **2018**, *25*, 15507−15517.
(37) Quan, Q.; Wen, H.; Han, S.; Wang, Z.; Shao, Z.; Chen, M. Fluorous-core nanoparticle-embedded hydrogel synthesized via tandem photo-controlled radical polymerization: Facilitating the separation of perfluorinated alkyl substances from water. *ACS Appl. Mater. Interfaces* **2020**, *12*, 24319−24327.
(38) Zhang, X.; Zhang, T.; Wang, Z.; Ren, Z.; Yan, S.; Duan, Y.; Zhang, J. Ultralight, superelastic, and fatigue-resistant graphene aerogel templated by graphene oxide liquid crystal stabilized air bubbles. *ACS Appl. Mater. Interfaces* **2019**, *11*, 1303−1310.
(39) Wang, X.; Nie, S.; Zhang, P.; Song, L.; Hu, Y. Superhydrophobic and superoleophilic graphene aerogel for ultrafast removal of hazardous organics from water. *J. Mater. Res. Technol.* **2020**, *9*, 667−674.
(40) An, H.; Li, Y.; Long, P.; Gao, Y.; Qin, C.; Cao, C.; Feng, Y.; Feng, W. Hydrothermal preparation of fluorinated graphene hydrogel for high-performance supercapacitors. *J. Power Sources* **2016**, *312*, 146−155.
(41) Zhao, M.; Deng, C. Fluorous modified magnetic mesoporous silica composites incorporated fluorous solid-phase extraction for the specific enrichment of N-linked glycans with simultaneous exclusion of proteins. *Talanta* **2016**, *159*, 111−116.
(42) Li, X.; Chen, S.; Li, L.; Quan, X.; Zhao, H. Electrochemically enhanced adsorption of nonylphenol on carbon nanotubes: Kinetics and isotherms study. *J. Colloid Interface Sci.* **2014**, *415*, 159−164.
(43) Zhao, B.; Liu, P.; Zhuang, H.; Jiao, Z.; Fang, T.; Xu, W.; Lu, B.; Jiang, Y. Hierarchical self-assembly of microscale leaf-like CuO on graphene sheets for high-performance electrochemical capacitors. *J. Mater. Chem. A* **2013**, *1*, 367−373.
(44) Du, Z.; Deng, S.; Chen, Y.; Wang, B.; Huang, J.; Wang, Y.; Yu, G. Removal of perfluorinated carboxylates from washing wastewater of perfluorooctanesulfonyl fluoride using activated carbons and resins. *J. Hazard. Mater.* **2015**, *286*, 136−143.
(45) Wang, F.; Liu, C.; Shih, K. Adsorption behavior of perfluorooctanesulfonate (PFOS) and perfluorooctanoate (PFOA) on boehmite. *Chemosphere* **2012**, *89*, 1009−1014.
(46) Elanchezhiyan, S. S. D.; Prabhu, S. M.; Kim, Y.; Park, C. M. Lanthanum-substituted bimetallic magnetic materials assembled carboxylate-rich graphene oxide nanohybrids as highly efficient adsorbent for perfluorooctanoic acid adsorption from aqueous solutions. *Appl. Surf. Sci.* **2020**, *509*, 144716.
(47) Huang, Y.; Zhang, W.; Bai, M.; Huang, X. One-pot fabrication of magnetic fluorinated carbon nanotubes adsorbent for efficient extraction of perfluoroalkyl carboxylic acids and perfluoroalkyl sulfonic acids in environmental water samples. *Chem. Eng. J.* **2020**, *380*, 122392.
(48) Li, X.; Chen, S.; Quan, X.; Zhang, Y. Enhanced adsorption of PFOA and PFOS on multiwalled carbon nanotubes under electrochemical assistance. *Environ. Sci. Technol.* **2011**, *45*, 8498−8505.
(49) Niu, Z.; Wang, Y.; Lin, H.; Jin, F.; Li, Y.; Niu, J. Electrochemically enhanced removal of perfluorinated compounds (PFCs) from aqueous solution by CNTs-graphene composite electrode. *Chem. Eng. J.* **2017**, *328*, 228−235.
(50) Sellaoui, L.; Guedidi, H.; Knani, S.; Reinert, L.; Duclaux, L.; Lamine, A. B. Application of statistical physics formalism to the modeling of adsorption isotherms of ibuprofen on activated carbon. *Fluid Phase Equilib.* **2015**, *387*, 103−110.
(51) Pang, X.; Bouzid, M.; dos Santos, J. M. N.; Gazzah, M. H.; Dotto, G. L.; Belmabrouk, H.; Bajahzar, A.; Erto, A.; Li, Z. Theoretical study of indigotine blue dye adsorption on $CoFe_2O_4$/

https://dx.doi.org/10.1021/acsomega.1c00044
ACS Omega 2021, 6, 7073−7085

chitosan magnetic composite via analytical model. *Colloids Surf., A* **2020**, *589*, 124467.
(52) Fagbayigbo, B. O.; Opeolu, B. O.; Fatoki, O. S.; Akenga, T. A.; Olatunji, O. S. Removal of PFOA and PFOS from aqueous solutions using activated carbon produced from Vitis vinifera leaf litter. *Environ. Sci. Pollut. Res.* **2017**, *24*, 13107−13120.
(53) Jun, B.-M.; Hwang, H. S.; Heo, J.; Han, J.; Jang, M.; Sohn, J.; Park, C. M.; Yoon, Y. Removal of selected endocrine-disrupting compounds using Al-based metal organic framework: Performance and mechanism of competitive adsorption. *J. Ind. Eng. Chem.* **2019**, *79*, 345−352.
(54) Deng, S.; Nie, Y.; Du, Z.; Huang, Q.; Meng, P.; Wang, B.; Huang, J.; Yu, G. Enhanced adsorption of perfluorooctane sulfonate and perfluorooctanoate by bamboo-derived granular activated carbon. *J. Hazard. Mater.* **2015**, *282*, 150−157.
(55) Kutsuna, S.; Hori, H.; Sonoda, T.; Iwakami, T.; Wakisaka, A. Preferential solvation of perfluorooctanoic acid (PFOA) by methanol in methanol-water mixtures: A potential overestimation of the dissociation constant of PFOA using a Yasuda-Shedlovsky plot. *Atmos. Environ.* **2012**, *49*, 411−414.
(56) Saeed, A.; Sharif, M.; Iqbal, M. Application potential of grapefruit peel as dye sorbent: kinetics, equilibrium and mechanism of crystal violet adsorption. *J. Hazard. Mater.* **2010**, *179*, 564−572.
(57) Schio, R. R.; Salau, N. P. G.; Malimann, E. S.; Dotto, G. L. Modeling of fixed-bed dye adsorption using response surface methodology and artificial neural network. *Chem. Eng. Commun.* **2020**, 1.
(58) Franco, D. S. P.; Duarte, F. A.; Salau, N. P. G.; Dotto, G. L. Analysis of indium (III) adsorption from leachates of LCD screens using artificial neural networks (ANN) and adaptive neuro-fuzzy inference systems (ANIFS). *J. Hazard. Mater.* **2020**, *384*, 121137.
(59) Simić, V. M.; Rajković, K. M.; Stojičević, S. S.; Veličlović, D. T.; Nikolić, N. Č.; Lazić, M. L.; Karabegović, I. T. Optimization of microwave-assisted extraction of total polyphenolic compounds from chokeberries by response surface methodology and artificial neural network. *Sep. Purif. Technol.* **2016**, *160*, 89−97.
(60) Franco, D. S. P.; Duarte, F. A.; Salau, N. P. G.; Dotto, G. L. Adaptive neuro-fuzzy inference system (ANIFS) and artificial neural network (ANN) applied for indium (III) adsorption on carbonaceous materials. *Chem. Eng. Commun.* **2019**, *206*, 1452−1462.
(61) Zou, X.; Zhang, H.; Chen, T.; Li, H.; Meng, C.; Xia, Y.; Guo, J. Preparation and characterization of polyacrylamide / sodium alginate microspheres and its adsorption of MB dye. *Colloids Surf., A* **2019**, *567*, 184−192.
(62) Brown, M. A.; Goel, A.; Abbas, Z. Effect of electrolyte concentration on the stern layer thickness at a charged interface. *Angew. Chem.* **2016**, *128*, 3854−3858.
(63) Yu, Q.; Zhang, R.; Deng, S.; Huang, J.; Yu, G. Sorption of perfluorooctane sulfonate and perfluorooctanoate on activated carbons and resin: Kinetic and isotherm study. *Water Res.* **2009**, *43*, 1150−1158.
(64) Meng, P.; Deng, S.; Lu, X.; Du, Z.; Wang, B.; Huang, J.; Wang, Y.; Yu, G.; Xing, B. Role of air bubbles overlooked in the adsorption of perfluorooctanesulfonate on hydrophobic carbonaceous adsorbents. *Environ. Sci. Technol.* **2014**, *48*, 13785−13792.
(65) Liu, K.; Zhang, S.; Hu, X.; Zhang, K.; Roy, A.; Yu, G. Understanding the adsorption of PFOA on MIL-101(Cr)-based anionic-exchange metal-organic frameworks: Comparing DFT calculations with aqueous sorption experiments. *Environ. Sci. Technol.* **2015**, *49*, 8657−8665.
(66) Xu, T.; Ji, H.; Gu, Y.; Tong, T.; Xia, Y.; Zhang, L.; Zhao, D. Enhanced adsorption and photocatalytic degradation of perfluorooctanoic acid in water using iron (hydr)oxides/carbon sphere composite. *Chem. Eng. J.* **2020**, *388*, 124230.
(67) Li, X.; Pignatello, J. J.; Wang, Y.; Xing, B. New insight into adsorption mechanism of ionizable compounds on carbon nanotubes. *Environ. Sci. Technol.* **2013**, *47*, 8334−8341.
(68) Yang, H.; Zhang, T.; Jiang, M.; Duan, Y.; Zhang, J. Ambient pressure dried graphene aerogels with superelasticity and multifunctionality. *J. Mater. Chem. A* **2015**, *3*, 19268−19272.
(69) Bhowmik, M.; Deb, K.; Debnath, A.; Saha, B. Mixed phase Fe_2O_3/Mn_3O_4 magnetic nanocomposite for enhanced adsorption of methyl orange dye: Neural network modeling and response surface methodology optimization. *Appl. Organomet. Chem.* **2018**, *32*, No. e4186.
(70) Foroutan, R.; Peighambardoust, S. J.; Mohammadi, R.; Omidvar, M.; Sorial, G. A.; Ramavandi, B. Influence of chitosan and magnetic iron nanoparticles on chromium adsorption behavior of natural clay: Adaptive neuro-fuzzy inference modeling. *Int. J. Biol. Macromol.* **2020**, *151*, 355−365.
(71) Li, Z.; Gómez-Avilés, A.; Sellaoui, L.; Bedia, J.; Bonilla-Petriciolet, A.; Belver, C. Adsorption of ibuprofen on organo-sepiolite and on zeolite/sepiolite heterostructure: Synthesis, characterization and statistical physics modeling. *Chem. Eng. J.* **2019**, *371*, 868−875.
(72) Atrous, M.; Sellaoui, L.; Bouzid, M.; Lima, E. C.; Thue, P. S.; Bonilla-Petriciolet, A.; Lamine, A. B. Adsorption of dyes acid red 1 and acid green 25 on grafted clay: Modeling and statistical physics interpretation. *J. Mol. Liq.* **2019**, *294*, 111610.

https://dx.doi.org/10.1021/acsomega.1c00044
ACS Omega 2021, 6, 7073−7085